

Arabidopsis COP1 guides stomatal response in guard cells through pH regulation

Seoyeon Cha ^{1,3}, Wang Ki Min^{1,3} & Hak Soo Seo ^{1,2} 

Plants rely on precise regulation of their stomatal pores to effectively carry out photosynthesis while managing water status. The *Arabidopsis* CONSTITUTIVE PHOTOMORPHOGENIC 1 (COP1), a critical light signaling repressor, is known to repress stomatal opening, but the exact cellular mechanisms remain unknown. Here, we show that COP1 regulates stomatal movement by controlling the pH levels in guard cells. *cop1-4* mutants have larger stomatal apertures and disrupted pH dynamics within guard cells, characterized by increased vacuolar and cytosolic pH and reduced apoplastic pH, leading to abnormal stomatal responses. The altered pH profiles are attributed to the increased plasma membrane (PM) H⁺-ATPase activity of *cop1-4* mutants. Moreover, *cop1-4* mutants resist to growth defect caused by alkali stress posed on roots. Overall, our study highlights the crucial role of COP1 in maintaining pH homeostasis of guard cells by regulating PM H⁺-ATPase activity, and demonstrates how proton movement affects stomatal movement and plant growth.

¹Department of Agriculture, Forestry and Bioresources, Research Institute of Agriculture and Life Sciences, Seoul National University, Seoul 08826, Republic of Korea. ²Bio-MAX Institute, Seoul National University, Seoul 08826, Republic of Korea. ³These authors contributed equally: Seoyeon Cha, Wang Ki Min. email: seohs@snu.ac.kr

Stomatal pores in leaves are surrounded by two guard cells and regulate gaseous exchange and water transpiration in plants. While the opening and closure of stomata are triggered by environmental factors such as light, temperature, and CO₂ concentration^{1,2}, their physical changes involve ionic movements, including K⁺, Cl⁻, and NO₃⁻³⁻⁵. These cations and anions constitute the buffer system inside the cell and participate in pH regulation alongside H⁺ exchanges, underscoring the significance of guard cell pH in stomatal movements⁶. To enhance photosynthesis and water use efficiency, a deeper understanding of guard cell pH regulation is crucial. Therefore, this study focuses on investigating the role of Arabidopsis CONSTITUTIVE PHOTOMORPHOGENIC 1 (COP1) in guard cell pH regulation, as it has been previously linked to regulating stomatal aperture and density for stomatal conductance⁷⁻⁹.

COP1 is a highly conserved E3 ubiquitin ligase in eukaryotes to ubiquitinate various protein substrates to consequently mark them for degradation¹⁰. In plants, COP1 serves as a central repressor of photomorphogenesis¹¹⁻¹³, and also regulates multiple pathways such as flowering time¹⁴, hormone signaling¹⁵, and circadian rhythm¹⁶. Particularly, in guard cells, COP1 negatively influences stomatal opening under the light and ABA signaling so that *cop1* mutants not only exhibit constitutively large and open stomata, also are insensitive to dark- and ABA-induced stomatal closure^{7,17}. Regarding the light signaling, COP1 acts downstream of CRY and PHOT to inhibit blue light-induced stomatal opening⁷ and also suppresses phyA/B-mediated red and far-red light-induced stomatal opening¹⁸, while stimulating stomatal closure under UV-B light perception^{19,20}. Additionally, COP1 promotes the ABA signaling pathway through the ubiquitination of PP2C family proteins and microtubule destabilization^{17,21}. This COP1-mediated degradation of PP2C leads to the release of the kinase OPEN STOMATA 1 (OST1), which activates Slow Anion Channels (SLAC1) and Quick Anion Channels (QUAC), whereas inactivating K⁺-inward rectifying channel (KAT1), leading to anion efflux and stomatal closure²²⁻²⁵. Indeed, *cop1* mutants display reduced SLAC1 channel activity, but no change in K⁺ channel activity²¹.

Despite the well-established role of COP1 in stomatal regulation, the underlying cellular mechanisms by which it affects guard cells *in vivo* that make *cop1* mutants so recalcitrant in responding to any environmental and endogenous signals to adjust the size of stomata are still an open question. It is conceivable to think of a common landscape that can embrace the light and ABA signaling in guard cells. Arabidopsis plasma membrane (PM) H⁺-ATPases, which pump out protons from the cytosol, are widely regarded as the final signaling destination for various pathways, such as in light, auxin, and immunity²⁶⁻³⁰. We thus here posit that pH serves as an important factor in stomatal guard cells generally applied for various stomatal responses. It is noteworthy that dominant mutants of ARABIDOPSIS H⁺-ATPASE 1 (AHA1), *ost2-2D*, which have constitutive activation of the PM H⁺-ATPase to open the stomata, are not responsive to ABA for the closure³¹. This insensitivity of *ost2-2D* mutants was recently corroborated by the detection of a higher cytosolic pH in their guard cells³², building on earlier research in 1992 that cytosolic pH change precedes stomatal closure³³. Cytosolic alkalinization has been implicated in both ABA-induced stomatal closure and fusicoccin (FC)-induced stomatal opening, making it difficult to uncover its homeostatic mechanism^{32,34,35}. Furthermore, vacuolar pH significantly affects stomatal regulation, with K⁺, Na⁺/H⁺ exchangers (NHX1/2) needed for alkalinization during opening³⁶ and V-PPase and V-ATPase necessary for acidification during closure³⁷⁻³⁹.

In this study, we aim to reassess how COP1 modulates stomatal movement in guard cells, with a particular emphasis on

cellular pH as a key biochemical factor for stomatal regulation. We investigate the altered pH dynamics in *cop1* mutants and examine how different pH levels affect stomatal physiology and plant growth, highlighting the importance of guard cell pH in integrating various signals to determine whether stomata should be open or closed.

Results

cop1 mutants exhibit distinct vacuolar dynamics in guard cells.

cop1 mutants have abnormally large stomatal apertures, causing a cooling effect on their leaf temperature due to the increased water transpiration¹⁷. Notwithstanding exposure to 72 h of darkness, ABA, flg22, and other abiotic stresses, the guard cells remain turgid⁴⁰, implying a potential issue with vacuolar dynamics, which directs stomatal movement through the turgor-driven mechanism. We therefore carried out examinations of their vacuolar properties in guard cells. Using the GFP-linked vacuolar H⁺-pyrophosphatase (V-PPase) as a tonoplast marker⁴¹, we first examined the vacuolar morphology of *cop1* mutants. Figure 1a shows the single and enlarged vacuoles of *cop1-4* mutants that occupied almost 80% of a single cell and represented a 1.4-fold increase in volume, compared to the several, separate vacuoles seen in WT, conferring larger stomatal apertures (Fig. 1b-d). This enlarged vacuolar morphology of *cop1-4* mutants was consistent under ABA treatment (Fig. 1a). Given the deviation of *cop1* mutants from the normal vacuolar volume range of wild-type, we surmised that the vacuolar pH in guard cells may also be altered.

To measure the vacuolar pH, we utilized the vacuole-specific loading dye, 2',7'-bis-(2-carboxyethyl)-5-(and-6)-carboxyfluorescein (BCECF), which changes its excitation peak based on pH^{36,42}. It exhibits maximum excitation spectra at 458 nm for acidic values and 488 nm for alkaline values. Therefore, we calculated the luminal pH of vacuoles ratiometrically expressed as 488/458 and converted it into the absolute pH values through a pH titration curve generated with guard cells. We incubated the epidermal peels in a series of buffers ranging from 4.3 to 7.8 (Supplementary Fig. 1). It is intriguingly noted that guard cells incubated in acidic buffers closed stomata and shrank, whereas those incubated in alkaline conditions opened stomata and swelled. These findings suggest that pH may have a causal impact on stomatal dynamics, with alkaline conditions leading to larger stomata. Further, we noted an unexpected nature of vacuolar pH during the development of guard cells⁴³. Young guard cells had acidic vacuoles that became alkaline as they matured (Supplementary Fig. 2). This observation supports the notion that V-PPase-mediated acidification is highly expressed in budding cells, promoting vacuolar and cellular expansion^{44,45}. Given these observations, we focused on mature guard cells with a cell length greater than 18 μm for subsequent analyses to rule out any developmental-dependent pH discrepancies.

We observed that *cop1-4* mutants have larger stomata with vacuoles that maintain an alkaline pH of 7.0, compared to WT with pH 6.8 (Fig. 1e, f). We further investigated the response of these vacuoles to ABA or dark treatments, and found that they did not undergo the expected vacuolar acidification required for stomatal closure³⁷. In contrast, WT vacuoles showed a decrease in pH of about 0.4–0.8 units in response to these treatments, while *cop1-4* only exhibited minor changes of about 0.1–0.3 units (Fig. 1e, f). This outcome suggests a deficiency in proton import into vacuoles in *cop1* mutants, which may explain their resistance to stomatal closure. The observed constitutively open and larger stomata in *cop1-4* mutants may be attributed to the higher pH of the single and occupied vacuoles. These distinct vacuolar properties of *cop1* mutants suggest the underlying signaling barriers that either inhibit or strengthen the regular pathway.

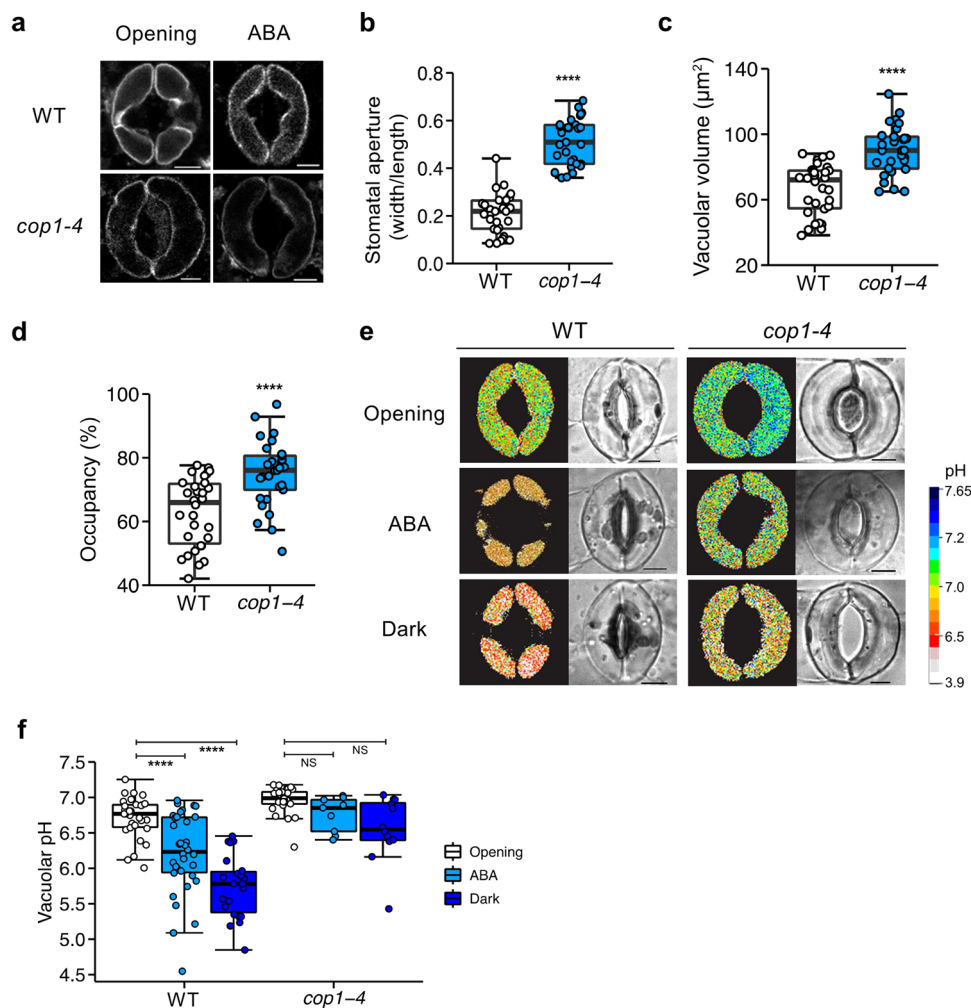


Fig. 1 *cop1-4* mutants exhibit altered vacuolar properties in guard cells. **a** Vacuolar structures in guard cells of wild-type (WT) and *cop1-4* mutants visualized with the tonoplast marker VACUOLAR H⁺-PYROPHOSPHATASE 1 (VHPI)-GFP after 2 h of light-induced stomatal opening, followed by treatment with or without 10 μM abscisic acid (ABA) for an hour. (Scale bar, 5 μm.) Quantitative analysis of three guard cell parameters after stomatal opening. Stomatal aperture index is calculated by dividing the stomatal width by its length (**b**), combined vacuolar volume (**c**), and vacuolar occupancy (**d**). Note that these were obtained from the same guard cells used in (**f**) for stomatal opening. *****P* < 0.0001; two-sample *t* test; *n* = 30 (WT) and *n* = 29 (*cop1-4*). Boxplots show the median (center line) and the 75th and 25th percentiles (edges of the box) of the data; whiskers extend to 1.5 times the interquartile range. **e** Representative pseudocolor ratiometric images of vacuolar pH in guard cells of wild-type (WT) and *cop1-4* mutants were obtained after 2 h of light-induced stomatal opening, followed by treatment with or without 10 μM ABA for 1 h, or 1 h of darkness. Guard cells were loaded with the pH-sensitive vacuolar loading dye 2',7'-bis-(2-carboxyethyl)-5-(and-6)-carboxyfluorescein (BCECF-AM), and the images were generated by dividing the emission images acquired in the 488 nm channel by those obtained in the 458 nm channel. Ratiometric images (left) and bright-field images (right). (Scale bar, 5 μm.) **f** Mean vacuolar pH values for entire vacuoles in guard cells of (**e**). *****P* < 0.0001 and NS, not significant (*P* > 0.05); two-way ANOVA; Tukey's HSD; *n* = 9–34.

Altered guard cell pH dynamics in *cop1* mutants. To gain a better understanding of the modified pH within vacuoles, we next profiled cytosolic pH through transgenic plants expressing ClopHensor, a genetically-encoded pH sensor³⁵, under various conditions modifying stomatal aperture (ABA, dark, and FC). This enabled us to monitor cytosolic pH *in vivo* at the single-cell level using a similar ratiometric calculation of the 488/458 ratio as that previously employed on BCECF. Together with *in vivo* calibration data (Supplementary Fig. 3), Fig. 2 illustrates that the basal levels of cytosolic pH were higher in *cop1-4* guard cells than in WT, as reflected by stronger signals detected at the 488 nm within the guard cell border. This result bolsters the link between cytosolic pH and stomatal aperture and is consistent with previous research demonstrating that *ost2-2D* mutants with constitutive stomatal opening have alkalinized cytosol in guard cells³². Elevated intracellular pH levels in guard cells of *cop1-4*

mutants indicate a homeostatic mechanism in which pH changes in the vacuole and cytosol occur in the same direction⁴⁶. After 10 min of ABA treatment, cytosolic pH of both WT and *cop1-4* mutants slightly increased (Fig. 2), while 1 h of ABA treatment to fully induce stomatal closure of WT resulted in cytosolic acidification in both plants (Supplementary Fig. 4). Dark treatment significantly reduced cytosolic pH of WT and *cop1-4* mutants, but still *cop1-4* mutants showed higher cytosolic pH than WT. Lastly, FC treatment induced cytosolic alkalinization for both WT and *cop1-4* mutants.

We then evaluated the apoplastic pH using the membrane-impermeable pH indicator 8-hydroxypyrene-1,3,6-trisulfonic acid trisodium salt (HPTS), whose pH is determined ratiometrically by 488/405 nm⁴⁷. A leaf disc was mounted in a stomatal opening buffer with HPTS added and immediately used for imaging. Combined with *in situ* HPTS calibration data (Supplementary

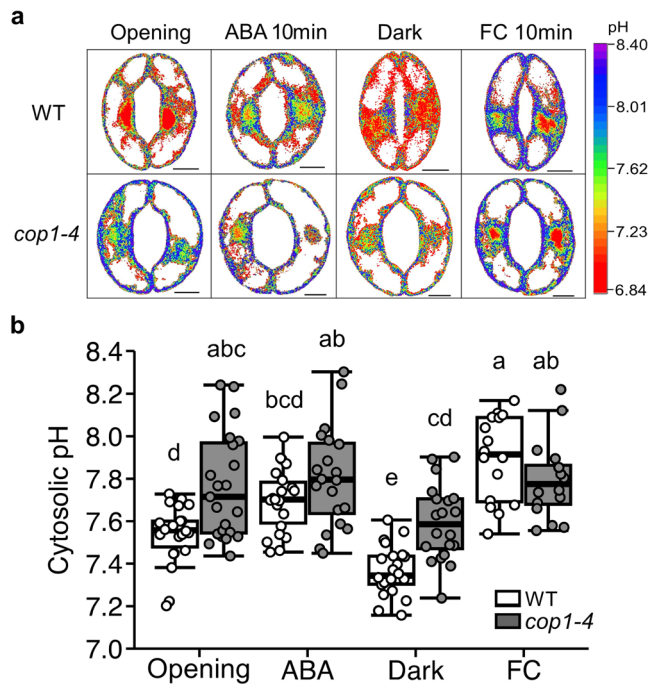


Fig. 2 Cytosolic pH of *cop1-4* mutants are more alkaline than WT.

a Representative pseudocolor ratiometric images of guard cells of wild-type (WT) and *cop1-4* mutants each expressing ClopHensor. Detached leaves were incubated with stomatal opening buffer for 2 h, and then treated with 10 μ M abscisic acid (ABA) for 10 min or with dark for 1 h. To assess the impact of fusicoccin (FC), dark-treated leaves were incubated with 10 μ M fusicoccin for 1 h. Fluorescence intensity of cytosolic pH in guard cells of WT and *cop1-4* mutants was measured directly from detached leaves using confocal laser scanning microscope (Leica SP8 X). Pseudocolor ratiometric images were generated by dividing the emission images obtained at 488 nm by those acquired at 458 nm. (Scale bar, 5 μ m.) **b** Quantification of ratiometric values for cytosolic pH in guard cells shown in (a). Different letters indicate statistically significant differences between the plants ($P < 0.05$); one-way ANOVA; Tukey's HSD.

Fig. 5), our results demonstrated that the apoplastic pH in *cop1-4* mutants was significantly lower than in WT, with an average difference of 0.13 units (Fig. 3a, c). This acidic apoplast, in contrast to the alkaline intracellular environment, creates a higher pH gradient across the guard cell in *cop1-4* mutants. This increased pH gradient may contribute to the constitutively open stomata phenotype in *cop1-4* mutants by affecting ion fluxes across the plasma membrane.

Given the acidic apoplastic space observed in *cop1-4* mutants, we investigated whether they follow the typical ABA signaling pathway characterized by a transient apoplastic alkalization⁴⁸. Short-term apoplastic pH increase is known to be involved in the plant stress response, such as to salinity, drought, and pathogen attack, and serves to initiate stomatal closure⁴⁹. Interestingly, it turned out that ABA-induced a prominent transient apoplastic alkalization in WT, resulting in a 0.13 pH unit increase, while the increase in apoplastic pH was minimal in *cop1-4* mutants (Fig. 3b, c). This dampened response to ABA may block or lower the extent of the normal progression of signaling required to stimulate stomatal closure in *cop1-4* mutants. Overall, the altered basal pH levels in *cop1-4* mutant guard cells demonstrate the role of COP1 in regulating pH and help to explain their insensitivity to various factors in the stomatal response.

COP1 acts negatively on proton pumping activity. We then sought to determine the underlying causes of the altered pH profiles in *cop1* mutants. We first analyzed the transcript levels of PM H^+ -ATPases, including *AHA1* and *AHA2*, but detected no significant changes (Supplementary Fig. 6). As the next possibility, we considered post-translational modifications and indirectly assayed proton pumping activity by incubating seedlings in MS media supplemented with bromocresol purple, a pH indicator dye that changes from purple to yellow as it becomes acidic. Our results showed enhanced proton extrusion in *cop1-4* mutant seedlings compared to WT, as manifested by the clear yellow color over the roots of mutants (Fig. 4a and Supplementary Fig. 7). Rhizosphere acidification was inhibited with Na_3VO_4 treatment in both WT and *cop1-4* mutants, indicating that PM H^+ -ATPase activity caused the proton extrusion in root cells

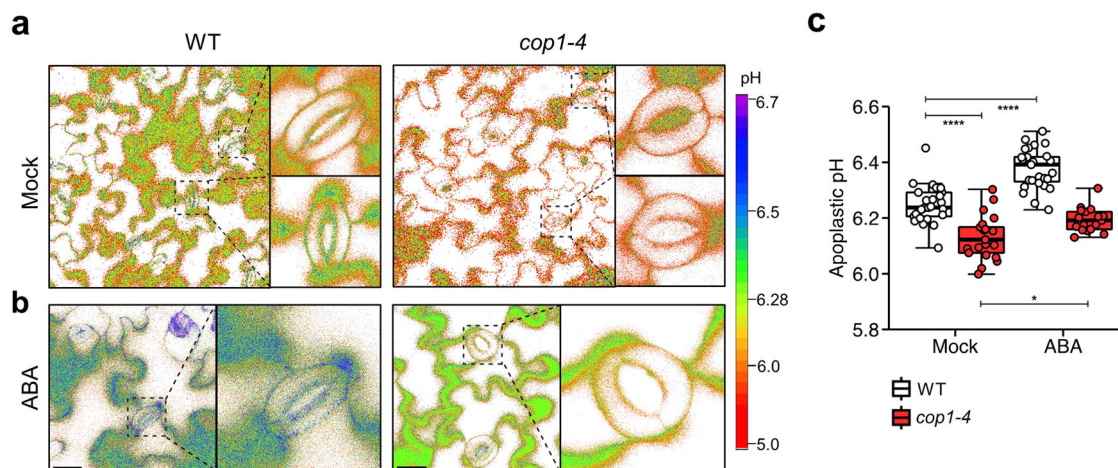


Fig. 3 *cop1-4* mutants exhibit constitutively acidic apoplast in leaf epidermal cells. **a, b** Representative pseudocolor images of apoplastic pH in the epidermis of wild-type (WT) and *cop1-4* mutants visualized using 8-hydroxypyrene-1,3,6-trisulfonic acid trisodium salt (HPTS) staining with or without abscisic acid (ABA) in the stomatal opening buffer. Staining and observation were conducted simultaneously and instantly. Ratiometric images were generated by dividing the emission images obtained in the 488 nm channel by those acquired in the 405 nm channel. Calculated values were converted into absolute pH values using the in situ HPTS calibration curve (Supplementary Fig. 3). Right panels show expansions of the left panels, respectively. (Scale bar, 20 μ m.) **c** Mean apoplastic pH values for guard cells shown in (a, b). **** $P < 0.0001$ and * $P < 0.05$; two-way ANOVA; Tukey's HSD; $n = 17$ to 27. Boxplots show the median (center line) and the 75th and 25th percentiles (edges of the box) of the data; whiskers extend to 1.5 times the interquartile range.

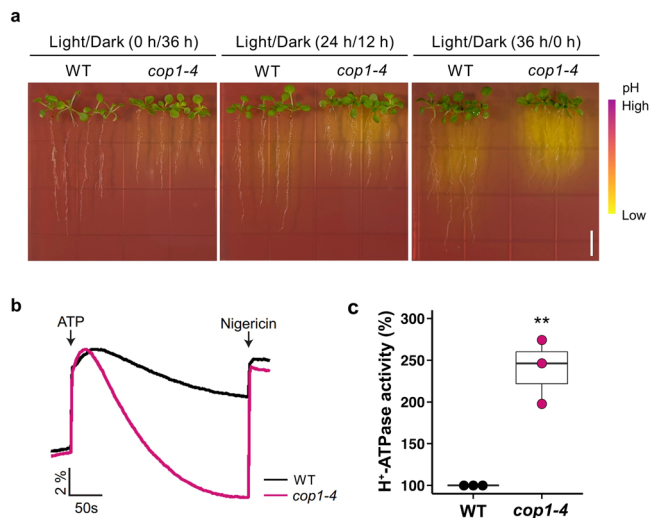


Fig. 4 COP1 negatively regulates proton pumping activities.

a Rhizosphere acidification assays were conducted using wild-type (WT) and *cop1-4* mutants. Eleven-day-old seedlings were transferred to $\frac{1}{2}$ MS media containing 0.003% of pH indicator dye bromocresol purple and grown vertically. Seedlings were then subjected to dark, long-day, and continuous light conditions, respectively, as indicated, and color changes were recorded after 36 h. (Scale bar, 1 cm.) The experiment was conducted three times, and one representative experiment is shown in **(a)**. **b** Plasma membrane H^+ -ATPase activity was measured using WT and *cop1-4* mutants. Plasma membrane vesicles were isolated from the leaves of WT and *cop1-4* mutant plants, and treated with reaction buffer containing pH-sensitive fluorescence probe quinacrine. H^+ -ATPase activation was induced by adding 3 mM ATP, and pH decrease inside the vesicles was measured using spectrofluorometer. Proton gradient inside the vesicles was collapsed by adding uncoupler nigericin. The experiment was conducted three times, and one representative experiment is shown in **(b)**. **c** Mean H^+ -ATPase activity of WT and *cop1-4* mutants of **(b)**. H^+ -ATPase activity of WT was set to 100%, and the relative H^+ -ATPase activity of *cop1-4* mutants was shown as percentage of the activity of WT. $**P < 0.01$; two-sample t-test; Boxplots show the median (center line) and the 75th and 25th percentiles (edges of the box) of the data; whiskers extend to 1.5 times the interquartile range.

(Supplementary Fig. 7). Moreover, both WT and *cop1-4* seedlings showed slightly lower proton extrusion level in MS media supplemented with ABA (Supplementary Fig. 7; upper panel) compared to control media, which is in line with other data (Fig. 3).

To further explore the role of COP1 in rhizosphere acidification, we questioned whether its effect on proton extrusion was dependent on light. We revealed that the degree of rhizosphere acidification was light-dependent in both *cop1-4* mutants and WT, gradually increasing as seedlings transitioned from complete darkness to continuous light over 36 h (Fig. 4a). This suggests that the PHOT-mediated blue light signaling pathway to activate PM H^+ -ATPases is not completely blocked by COP1, despite its known downstream function⁷. In light of *cop1-4* displaying increased acidification even under continuous light, we rather concluded that COP1 quantitatively inhibits the blue light signaling pathway by controlling the stability of downstream components⁵⁰.

Based on rhizosphere acidification assay, we speculated that *cop1-4* mutants may have enhanced proton pumping activity also in the shoot part, where the guard cells reside. To directly measure PM H^+ -ATPase activity of *cop1-4* mutants, we isolated PM vesicles from the rosette leaves of WT and *cop1-4* mutants with aqueous two-phase separation method⁵¹. Each PM vesicles

harboring same amount of PM H^+ -ATPase protein (Supplementary Fig. 8) was subjected to PM H^+ -ATPase activity measurement using pH-sensitive fluorescence probe quinacrine^{51,52}. The results clearly demonstrated that *cop1-4* mutants have about 2.5-fold higher PM H^+ -ATPase activity than WT (Fig. 4b, c). Together with the rhizosphere acidification assay, these data strongly indicate that COP1 negatively regulates proton pumping activity.

Enhanced PM H^+ -ATPase activity contributes to stomatal opening and alkaline tolerance of *cop1-4* mutants. As *cop1-4* mutants had higher PM H^+ -ATPase activity than WT, we asked whether PM H^+ -ATPase activity is the key factor for constitutive stomatal opening phenotype of *cop1-4* mutants. To investigate this, we treated guard cells of WT and *cop1-4* mutants with sodium orthovanadate (Na_3VO_4), a PM H^+ -ATPase inhibitor, and compared the stomatal aperture with ABA, dark, and FC-treated guard cells. It was observed that Na_3VO_4 -treated *cop1-4* mutants showed reduced stomatal aperture to the similar extent of light-treated WT, just as ABA-treated *cop1-4* mutants (Fig. 5a, b). On the other hand, unlike WT, dark treatment could not induce stomatal closure of *cop1-4* mutants, and subsequent FC treatment also did not open the stomata. These results indicate that stomata of *cop1-4* mutants are insensitive to dark-induced stomatal closure and FC-induced stomatal opening, and blocking PM H^+ -ATPase activity is sufficient to restore constitutive open stomata phenotype of *cop1-4* mutants.

PM H^+ -ATPases pump intracellular proton out of the cell, thereby generating electrochemical proton gradient across PM and mediating various physiological responses such as salt and alkali tolerances^{53,54}. Enhanced PM H^+ -ATPase activity of *cop1-4* had prompted us to investigate alkali tolerance of *cop1-4* mutants, as salt tolerance of *cop1-4* mutants was described previously⁵⁵. We generated MS media with pH of 3.6, 5.8, and 8.0, and then transferred 11-day-old WT and *cop1-4* seedlings. After grown vertically for 7 days, we observed that both WT and *cop1-4* mutants grown in pH 8.0 exhibited reduced fresh weight compared to pH 5.8, but this decrease was smaller in *cop1-4* mutants (Fig. 5c, d). Meanwhile, primary root length of WT and *cop1-4* mutants grown in pH 8.0 showed no significant differences. These data suggest that enhanced PM H^+ -ATPase activity confers alkaline tolerance to *cop1-4* mutants, especially resistance to alkalinity-driven growth inhibition.

Discussion

Arabidopsis COP1 is a central light signaling repressor that suppresses stomatal opening in guard cells by inhibiting light-induced opening and promoting ABA-induced closure (Fig. 6). Our study identified a new function of COP1 in pH regulation that converges light and ABA signaling pathways to control stomatal movement. We found that constitutive stomatal opening in *cop1* mutants was associated with significant alkalization of vacuoles and cytosol, coupled with acidification of the apoplast, indicating altered basal pH levels in guard cells (Figs. 1, 2, and 3). This observation aligns with previous research showing that pH changes inside the vacuole and cytosol typically occur in the same direction⁴⁶. It is intriguing that mutations in genes other than pumps or channels can affect pH levels. For instance, mutations in the TMK1, a gene involved in auxin signaling, led to higher apoplastic pH levels due to its direct phosphorylation and activation of PM H^+ -ATPases^{27,56}. In our study, we demonstrated that COP1 negatively regulates the activity of PM H^+ -ATPases (Fig. 4), shedding light on the mechanism by which COP1 controls intracellular pH and ultimately governs stomatal movement and plant growth as to light.

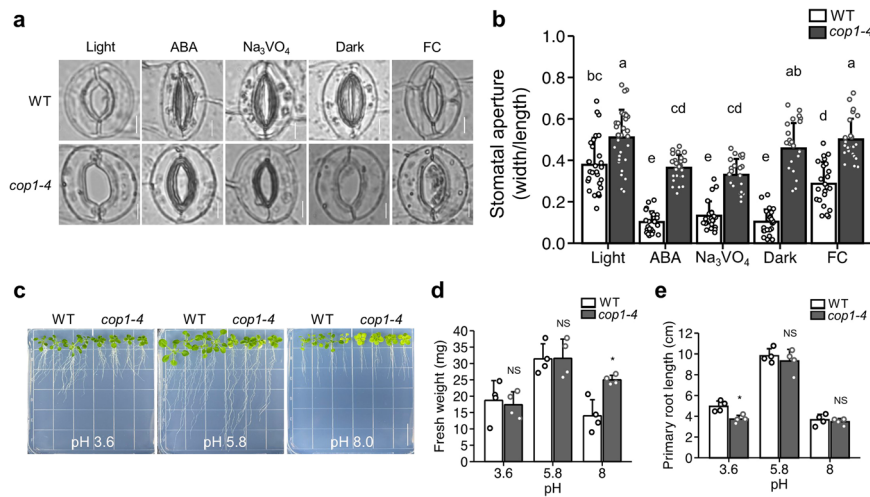


Fig. 5 Enhanced plasma membrane (PM) H⁺-ATPase activity of *cop1-4* mutants affects plant growth and stomatal behavior. **a** Detached leaves of 11-day-old wild-type (WT) and *cop1-4* mutant seedlings were incubated with stomatal opening buffer for 2 h, and then treated with various conditions as Fig. 2, except for abscisic acid (ABA) treated for 1 h. Guard cells were incubated with 1 mM Na₃VO₄ to investigate the role of H⁺-ATPase on stomatal aperture. (Scale bar, 5 μm.) **b** Quantification of stomatal apertures of guard cells from (a). Stomatal aperture index calculated by dividing the stomatal width by its length. Different letters indicate statistically significant differences between the plants ($P < 0.05$); one-way ANOVA; Tukey's HSD. **c** 11-day-old seedlings of WT and *cop1-4* mutants were transferred to ½ MS media at varying pH levels (3.6, 5.8, and 8.0) and grown vertically. Photographs and physiological assays were conducted 7 days after transferring. (Scale bar, 2 cm.) **d, e** Corresponding quantification of fresh weight (**d**) and primary root length (**e**) of plants from (c). * $P < 0.05$ and NS, not significant ($P > 0.05$); two-sample *t* test; $n = 4$ each.

The constitutive opening of stomata with larger apertures in *cop1* mutants indicates that COP1 plays a negative role in stomatal opening. This phenotype was further characterized by expanded vacuoles with higher alkalinity compared to WT guard cells (Fig. 1). Two disrupted pH signaling mechanisms are attributable to the impaired stomatal closure of *cop1* mutants upon ABA treatment: the highly alkalized cytosol and acidified apoplast diminish the effectiveness of conveying external signals into the vacuoles (Fig. 2, 3), and the vacuoles fail to undergo acidification for volume reduction (Fig. 1)^{32,37,49}. Our experiments showed that guard cells around ABA-treated closed stomata display vacuolar acidification (Fig. 1), cytosolic acidification (Supplementary Fig. 4), and apoplastic alkalization (Fig. 3). In the case of *cop1-4* mutants, they maintained alkaline vacuole (Fig. 1) and cytosol (Fig. 2 and Supplementary Fig. 4), and acidified apoplast (Fig. 3), which showed the opposite pH profiles with closed stomata.

The increase of cytosolic pH in *cop1-4* mutants is consistent with the phenotype of *slac1-1* mutants, which are also defective in ABA-induced stomatal closure due to impaired anion loss from the cytosol⁶. Moreover, *cop1-4* mutants show a minor increase in apoplastic pH compared to WT with ABA treatment, which hinders the increase in ABA concentration under stress conditions. Normally, the apoplast alkalizes under stress conditions, which helps increase the ABA concentration⁴⁹. The increased intracellular pH and decreased intercellular pH observed in *cop1-4* mutants could either be a cause or a consequence of their constantly photomorphogenic traits, and it is similar to the pH profile observed in photosynthesis-activating cells in response to light exposure in plants^{46,57}.

In this study, we observed stable cytosolic pH of *cop1-4* mutants upon ABA, dark, and FC treatment (Fig. 2). It was previously reported that 10 min of ABA treatment induces cytosolic alkalization^{32,37}, which pH dynamic is opposite to dark-induced cytosolic acidification (Fig. 2). Our experiment also resulted in similar cytosolic alkalization after 10 min of ABA treatment (Fig. 2), but prolonged ABA treatment about 1 h was sufficient to close the WT stomata and resulted in cytosolic

acidification (Supplementary Fig. 4). A study that treated ABA for 1 day also reported diminished PM H⁺-ATPase activity⁵⁸. Here, we speculate that at the early stage of ABA signaling (about 0–10 min after ABA treatment), PM H⁺-ATPases are activated to induce pH gradient across the PM³⁷, but after sufficient signal transduction (about 1 h after ABA treatment), PM H⁺-ATPase activity decreases and induces cytosolic acidification and apoplastic alkalization.

In the case of *cop1-4* mutants, basal pH of vacuole and cytosol are higher, and that of apoplast is lower than WT. This profile is maintained even after ABA or dark treatment, and vacuolar morphology and intracellular pH were even unchanged upon those treatments. Based on our observations about disrupted pH profiles of *cop1-4* mutants, we suspected that acidic apoplast and alkaline cytosol may be due to activation of PM H⁺-ATPases, ion pumps that export cellular protons out of the cells. Previous studies showed that activating or overexpressing PM H⁺-ATPases induced stomatal opening^{31,59}, which support the relationship between COP1 and PM H⁺-ATPases. Our rhizosphere acidification assay (Fig. 4a and Supplementary Fig. 7) and direct PM H⁺-ATPase activity assay (Fig. 4b, c) suggested that COP1 inhibits the proton pumping activity of PM H⁺-ATPases, which are primarily responsible for pH regulation stimulated by blue light (Fig. 4). This mechanism confirms the existing knowledge of the downstream function of COP1, which represses the PHOT-mediated blue light signaling pathway. It is worth noting that COP1 does not completely block the blue light signaling pathway, but rather regulates it quantitatively (Fig. 4). Supporting this is the observation that, cotyledon expansion is gradually reduced with an increase in COP1 amount under blue light⁵⁰. The antagonistic relationship between COP1 and H⁺-ATPases is further embodied in a phenotypic way. Increased proton extrusion due to the hyperactivation of H⁺-ATPases results in enlarged stomata and lower leaf temperatures¹⁷. These effects are similar to those seen in *ost2-2D* and *AHA1*-overexpressing plants, reinforcing the role of COP1 in regulating H⁺-ATPases and affecting pH^{31,59}. While COP1 is conventionally known for its activities in the nucleus, recent evidence shows that a significant

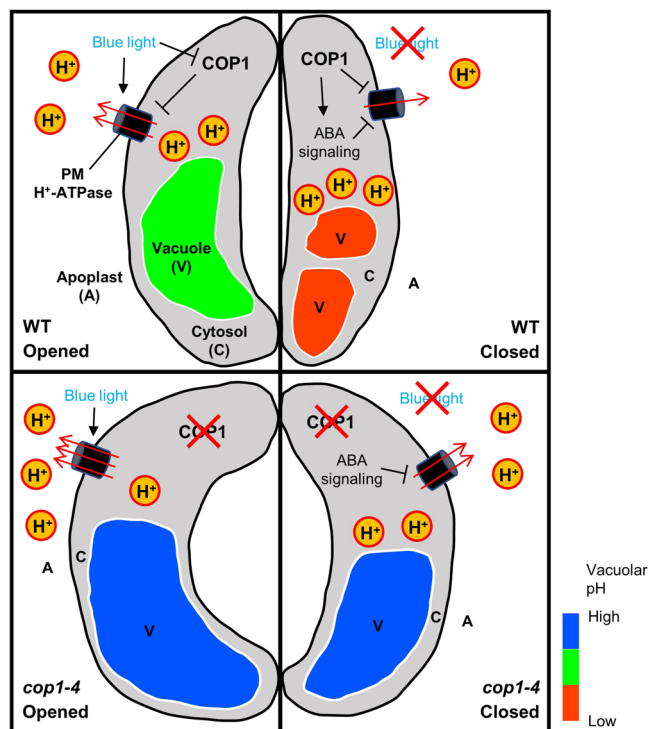


Fig. 6 A hypothetical model for the role of COP1 in regulating stomatal movement through pH regulation.

In an opened wild-type (WT) guard cell (upper left panel), proton pumping by plasma membrane (PM) H^+ -ATPase is downregulated by COP1. After stomata-closing signals such as ABA or dark (upper right panel), COP1 promotes ABA signaling, thereby inactivating PM H^+ -ATPase activity again. Thus, cytosolic acidification and apoplastic alkalization occur, and subsequent signal transduction induces vacuolar acidification and fragmentation, and finally stomatal closure. In an opened guard cell of *cop1-4* mutant (lower left panel), absence of COP1 is responsible for enhanced PM H^+ -ATPase activity. This elevated activity results in acidic apoplast and alkaline cytosol compared to WT. Stronger pH gradient across the PM induces signaling for stomatal opening, followed by enlarged alkaline vacuole and constitutive open stomata phenotype of *cop1-4* mutants. After ABA or dark-mediated stomatal closure signals (lower right panel), only mild inhibitory effect can be posed to PM H^+ -ATPase due to absence of COP1, a positive regulator of ABA signaling. Therefore, *cop1-4* mutant's apoplastic pH is lower, and cytosolic pH remains higher than WT guard cells with closed stomata. Still, pH gradient across the PM is sufficient to induce stomatal opening, and the vacuole morphology and pH remain unaffected. Black arrows indicate stimulation, and blocked lines indicate inhibition. Red arrows indicate proton (H^+) movement. Relative pH of cytosol and apoplast are proportional to the numbers of " H^+ "s inside respective regions. For graphical visibility, vacuoles at the upper side of the guard cells are omitted.

portion of COP1 is localized outside of the nucleus⁶⁰, and its activity in the cytosol has also been uncovered⁶¹. One possible molecular mechanism for the regulation of H^+ -ATPases by COP1 involves ubiquitination of the H^+ -ATPase protein through its E3 ligase activity, similar to yeasts⁶². Alternatively, COP1 may target 14-3-3 proteins, which are crucial for H^+ -ATPase activation, to interrupt forming a stable complex with H^+ -ATPase⁶³. COP1's role in ABA signaling may be another possibility. COP1, as an E3 ubiquitin ligase, positively regulates ABA signaling via ubiquitination and degradation of clade A type 2 C phosphatases (PP2C) ABI/HAB and AHG3¹⁷. ABA signaling pathway also participates in regulating PM H^+ -ATPase activity. ABA induces BRI1-ASSOCIATED RECEPTOR KINASE 1 (BAK1) phosphorylation and subsequent activation of AHA2³², or inhibiting

Protein Phosphatase 1 (PP1) in *Vicia faba*, which mediates phosphorylation and activation of PM H^+ -ATPases⁶⁴. Further studies regarding direct connection between COP1, ABA signaling components and PM H^+ -ATPases should be addressed.

Application of PM H^+ -ATPase inhibitor to the guard cells efficiently induced stomatal closure of both WT and *cop1-4* mutants, to the similar extent with ABA, which implies PM H^+ -ATPases' significant role in stomatal movement (Fig. 5a, b). During stomatal opening process activated by blue light, photoreceptors mediate phosphorylation and activation of PM H^+ -ATPases in guard cells^{26,65,66}. Activated PM H^+ -ATPases pump the protons out of the cells, thereby generating electrochemical gradient across the PM. This gradient induces the uptake of cations such as K^+ , followed by anion accumulation in the cytosol⁶⁷. Higher ion concentration results in increased water entry and turgor pressure, finally opening the stomata. To our experiments, *cop1-4* mutants, with enhanced PM H^+ -ATPase activity, maintain strong pH gradient ($pH_{\text{cyt}} - pH_{\text{apo}}$) of about 1.6 pH unit, while that of WT was about 1.3 unit (Figs. 2, 3). Established pH gradient across the PM may contribute to enhanced K^+ uptake by potassium channels⁶⁸, upregulating stomatal opening process mentioned above. Acidic apoplast can also attribute to open stomata phenotype of *cop1-4* mutants. Acid-growth theory states that proton extrusion-induced apoplastic acidification promotes cell expansion via activating cell wall loosening enzymes, which can make cells bigger through their turgor pressure^{69,70}. Even under ABA treatment, guard cells of *cop1-4* mutants exhibited more acidic apoplast than WT, and vacuole morphology and pH were unchanged, which explain *cop1-4* mutants' insensitivity towards ABA (Figs. 2, 3). ABA treatment and Na_3VO_4 treatment could not induce full closure of *cop1-4* stomata, and we carefully speculate that this is due to vacuole inflexibility of *cop1-4* mutants. The specific mechanism of how COP1 regulates vacuolar morphology and pH is largely unknown yet. One possible mechanism will be that COP1 can directly regulate tonoplast-residing ion pumps such as V-ATPases or V-PPases, which participate in guard cell signal transduction⁶⁷. Other possibility may be that modified pH gradient across the tonoplast because of highly alkalized cytosol can contribute to impaired signal transduction or enzymatic activity of tonoplast proteins⁷¹. Na_3VO_4 , which is a phosphate analog, inhibits the activities of enzymes requiring phosphate compounds, such as P-type ATPases including PM H^+ -ATPases and protein tyrosine phosphatases (PTPs)^{72,73}. As Arabidopsis has several P-type ATPases and PTPs mediating ion transport and signal transduction, inhibition of those proteins with Na_3VO_4 may affected our *in vivo* experiments, resulting in incomplete stomatal closure of *cop1-4* mutants. Indeed, previous study showed that inhibiting the activity of PTPs prevented stomatal closure after various stomata-closing cues⁷³. Still, combined with our results (Figs. 1–4) and previous studies emphasizing important roles of PM H^+ -ATPases on stomatal responses, we assume that elevated activity of PM H^+ -ATPases is responsible for abnormal stomatal responses of *cop1-4* mutants, even side effects of Na_3VO_4 may exist.

Owing to their high PM H^+ -ATPase activity, *cop1-4* mutants display tolerance to root-induced alkali stress in the context of fresh weight (Fig. 5c–e). Previously, it was reported that SOS3-LIKE CALCIUM BINDING PROTEIN 3 (SCaBP3)/CALCI-NEURIN B-LIKE 7 (CBL7) directly binds to AHA2 and promote autoinhibition of H^+ -ATPase activity⁵⁴. After alkali stimuli, SCaBP3/CBL7 is disassociated with AHA2 and subsequent increased H^+ -ATPase activity enhances alkali tolerance. Indeed, mutation of SCaBP3/CBL7 caused increase in PM H^+ -ATPase activity and alkali tolerance⁵⁴. Moreover, root-specific activation of OST2/AHA1 resulted in plant growth and nutrient

accumulation in shoot⁷⁴. COP1 may also participate in these processes by negatively regulating PM H⁺-ATPase activity, mediating pH dynamics of cells and physiological responses under various stress conditions.

Regulating intracellular pH is vital for eukaryotic cells because it affects enzyme activities and protein modification, and maintaining it within physiological ranges is essential⁷⁵. To cope with volatile environments, plants, as sessile organisms, have evolved to acquire vacuoles that provide greater buffering capacity, and have conserved two major proton pumps, PM H⁺-ATPases and V-PPase, across plant taxa⁷⁶. However, dysregulated pH in *cop1-4* mutants with constitutively increased cytosolic pH and decreased apoplastic pH is reminiscent of cancer cells that capitalize on an alkaline intracellular pH for cell proliferation and apoptosis evasion while consuming more glucose⁷⁷. Similarly, *cop1* mutants exhibit higher biomass and increased sucrose uptake⁵⁵, finding parallels in cancer cells with respect to constitutive growth and elevated pH gradient. Thus, the pH gradient, as a ubiquitous energy source, is critical for cellular activities across organisms for biological growth and maintenance. This study provides physiological evidence for the role of COP1 in pH regulation to modulate plant growth and offers a perspective on the intricate mechanisms of pH-dependent cellular behavior.

Materials and methods

Plant materials and growth conditions. All mutants and transgenic *A. thaliana* plants were from the Columbia-0 (Col-0) ecotype background and *cop1-4* were used in this study⁷⁸. Col-0 was used as WT for all experiments. T3 homozygous plants of the *pUBQ10::ClopHensor* transgenic lines (Col-0 and *cop1-4* background)³⁵, were used for assays.

Seeds were surface-sterilized with 70% ethanol, sown on half-strength Murashige and Skoog (1/2 MS) medium containing 1% sucrose and 0.6% plant agar (pH 5.8), stratified in the dark at 4 °C for 3 days, and then grown under long-day conditions (16 h light/8 h dark) at 22 °C and 60% relative humidity in growth chambers. Unless otherwise stated, 8-day-old seedlings were transferred to and grown on soil as one plant per pot (6 cm in length and height) under short-day conditions (8 h light/16 h dark) at 22 °C and 60% relative humidity in environmentally controlled growth chambers. Four-week-old plants were used for experiments, unless otherwise noted.

For the phenotypic analysis of plants grown on media with varying pH, 11-day-old plants grown horizontally were transferred to half-strength MS medium with the varying pH levels (3.6, 5.8, 8.0) that were adjusted with 2.5 mM MES-BTP, except for the pH 3.6 medium. To prepare the pH 3.6 medium, agar-containing medium was later mixed with MS medium after autoclaving due to agar hydrolysis at low pH. After transferring the seedlings to the manipulated pH medium, they were grown vertically for an additional 7 days. All physiological results were obtained with 18-day-old plants.

Imaging and measuring cellular pH. Imaging and measuring cellular pH were conducted using the Leica SP8 X confocal laser scanning microscope equipped with a HC PL APO CS2 x40 water immersion objective.

To measure vacuolar pH in guard cells, the fluorescent cell-permeant dye BCECF-AM (Molecular Probes) was used with slight modifications^{36,42}. Specifically, dye loading was achieved by submerging the epidermal peels in stomatal opening buffer (5 mM MES-BTP (pH 6.5), 50 mM KCl, 100 μM CaCl₂) with 10 μM BCECF-AM and 0.02% Pluronic F-127 (Invitrogen) to facilitate dye loading, followed by 90 min of staining at 22 °C in darkness. After staining, the epidermal peels were washed once in

dye-free buffer. The peels were then incubated in stomatal opening buffer for 2 h in light at 22 °C and either directly imaged or treated with 10 μM ABA for 1 h or darkness for 1 h. Fluorescence signals for protonated BCECF (excitation, 458 nm; emission, 514 nm) and deprotonated BCECF (excitation, 488 nm; emission, 514 nm) were detected. The ratio (488/458) was then converted into absolute pH values based on the calibration curve (Supplementary Fig. 1). In vivo calibration of BCECF was performed in guard cells, which were incubated for 30 min in pH equilibration buffers containing 50 mM citrate buffer-BTP (pH 4.3–5.0), 50 mM MES-BTP (pH 5.0–6.3) or 50 mM HEPES-BTP (pH 6.3–7.8) and 100 μM nigericin (Sigma-Aldrich). Ratio values were plotted against pH, and the calibration curves were generated from log-transformed polynomial regression using R software.

Guard cell cytosolic pH was measured through genetically-encoded pH sensors using plants expressing *pUBQ10::ClopHensor*³⁵. Intact leaves were mounted on the slide glass and instantly used for imaging. Fluorescence signals for protonated one (excitation, 458 nm; emission, 514 nm) and deprotonated one (excitation, 488 nm; emission, 514 nm) were detected, and the relative cytosolic pH was calculated by 488/458. For in vivo calibration of ClopHensor, guard cells of WT expressing ClopHensor were incubated for 30 min in pH equilibrium buffers containing 50 mM HEPES-BTP (pH 6.3–7.8) and 50 mM ammonium acetate³⁵. Ratio values were plotted against pH, and the calibration curves were generated from linear regression using R software.

Apoplastic pH measurement was performed using a ratio-metric fluorescent dye HPTS⁴⁷. Intact leaves were mounted on a block of solid stomatal opening buffer described above supplemented with 1 mM of 8-hydroxypyrene-1,3,6-trisulfonic acid trisodium salt (HPTS; Alfa Aesar) and instantly used for imaging. Fluorescence signals for the protonated HPTS (excitation, 405 nm; emission, 514 nm) and deprotonated HPTS (excitation, 488 nm; emission, 514 nm) were detected. In situ calibration of HPTS was performed with pH equilibration buffers used for in vivo BCECF calibration containing 1 mM of HPTS. Ratio values were plotted against pH, and the calibration curves were generated from log-transformed linear regression.

pH imaging analysis. Fiji software was used to analyze the images with batch processing from a custom ImageJ macro. Manual thresholding was applied to mask and remove noise signals. To calculate the relative pH, the pixel value of the deprotonated signal was divided by that of the protonated signal. The ratio values were represented using a color lookup table, with the same minimum and maximum values set for each experiment, NA values for white color. The relative pH values were transformed into absolute pH values using the equation derived from the calibration curve. Calculated values were averaged over a pair of guard cells and statistically evaluated in R.

Vacuolar analysis. Guard cell vacuolar morphology was assessed using the *pVHP1::VHP1-sGFP* transgenic lines expressing the tonoplast marker⁴¹. GFP fluorescence was excited at 488 nm with an emission band of 500–500 nm. To estimate vacuolar volume, the BCECF dye was used as a vacuolar loading dye, and vacuolar occupancy was calculated as the ratio of vacuolar volume to the guard cell volume.

Rhizosphere acidification assay. 11-day-old plants, initially grown horizontally, were transferred to half-strength Murashige and Skoog (MS) medium (1 mM MES-KOH, pH 6.3), supplemented with 0.003% bromocresol purple, 1% sucrose, and 0.8% plant agar, and grown vertically for 36 h in growth chamber with

the noted condition. In the case of additional treatments, a 4 mM Na₃VO₄ medium was prepared using a 200 mM sodium orthovanadate (Sigma-Aldrich) stock solution (pH 9.4), while a 10 μM abscisic acid (ABA) medium was from a 10 mM ABA stock. No further pH adjustment was undertaken while preparing the Na₃VO₄ medium using KOH. The plates were visually examined and the color was evaluated.

Plasma membrane vesicle isolation. Plants were grown in potting soil in a growth chamber under long-day conditions (16 h light/8 h dark) at 22 °C and 60% relative humidity. Three-week-old plant materials were prepared for isolating plasma membrane vesicles using the aqueous two-phase separation method⁵¹. Fresh plants were homogenized with an ice-cold homogenization buffer (0.33 M sucrose, 10% (v/v) glycerol, 0.2% BSA, 0.2% casein hydrolysate, 0.6% (w/v) polyvinylpyrrolidone, 5 mM ascorbic acid, 5 mM EDTA, 5 mM dithiothreitol (DTT), 1 mM phenylmethylsulfonyl fluoride (PMSF), 1× protease inhibitor and 50 mM HEPES-KOH, pH 7.5). The homogenate was filtered through two layers of Miracloth and centrifuged at 13,000 g for 10 min. The supernatant was then centrifuged at 100,000 g for 1 h to obtain a microsomal pellet that was resuspended in buffer I (0.33 M sucrose, 3 mM KCl, 1 mM DTT, 0.1 mM EDTA, 1× protease inhibitor, and 5 mM potassium phosphate, pH 7.8). The PM (upper phase) was obtained using pre-cold two-phase mixture (6.2% (w/w) Dextran T-500 and 6.2% (w/w) polyethylene glycol 3350 in 5 mM potassium phosphate (pH 7.8), 0.33 M sucrose, and 3 mM KCl) by centrifuging the tubes at 1000 g for 5 min, repeating three times to obtain the milky-white and transparent upper phase. The final upper phases were collected and diluted with buffer II (0.33 M sucrose, 0.1 mM EDTA, 1 mM DTT, 1× protease inhibitor, 20 mM HEPES-KOH, pH 7.5), and then centrifuged at 100,000 g for 1 h. The resulting pellet was collected and resuspended with buffer II containing 1 mM EDTA to obtain the PM.

PM H⁺-ATPase activity assay. The isolated PM vesicles were used to measure the H⁺-transport activity^{51,52}. The H⁺ produced by PM H⁺-ATPase from inside-out vesicles formed an inside-acid pH gradient (pH) in the vesicles, and it was measured as a decrease (quench) in the fluorescence by a pH-sensitive fluorescence probe quinacrine (Sigma-Aldrich). Fifty micrograms of PM vesicles were incubated with 2 ml of reaction buffer (140 mM KCl, 3 mM MgSO₄, 5 μM quinacrine, 0.05% (w/v) Brij-58, and 20 mM HEPES-BTP, pH 7.0) for 5 min in the darkened chamber of a spectrofluorometer (FP-8500) with 430 nm excitation and 500 nm emission wavelength. After the fluorescence was stabilized, the reaction was initiated by adding 3 mM ATP (final concentration) and the fluorescence was recorded for 5 min. At the end of the reaction, 10 μM (final concentration) protonophore nigericin was added to the assay buffer to dissipate the pH gradient and stop the reaction.

Examination of PM H⁺-ATPase protein levels. The isolated PM vesicle samples of WT and *cop1-4* mutants were subjected to SDS-PAGE. Following 8% SDS-PAGE, PM H⁺-ATPase protein levels were examined by western blotting with anti-PM H⁺-ATPase antibody (AS07-260; Agrisera). The same PVDF membrane used in the western blotting was stained with Coomassie Brilliant Blue, which was used as a loading control.

Quantitative RT-PCR. Total RNA was extracted from 14-d-old seedlings using the Plant Total RNA Purification Mini kit (Favorgen) according to the manufacturer's protocol. RNA was then diluted to 10 ng/μl and reverse-transcribed into cDNA using the ReverTra Ace qPCR RT Master Mix with gDNA Remover

(TOYOBO). qRT-PCR was performed using the TOPreal qPCR PreMIX kit (Enzynomics) in a 20 μl reaction on a Real-Time PCR LightCycler 480 System (Roche). Gene-specific primers were designed for *AHA1* (forward: 5'-GGACAAAGTTCGGTGTGAGGT3', reverse: 5'-ACCAACTCCTTGACCTGGTG-3') and *AHA2* (forward: 5'-TGCTCAAAGGACACTTCACG-3', reverse: 5'-GCCCTTAGCTTCACGACTG-3'). Relative expression values were determined using *UBQ10* (forward: 5'-GGCCTTGTATAATCCCTGATGAATAAG-3', reverse: 5'-AAAGAGATAACAGGAACGGAAACATAGT-3') as an internal reference and the comparative Ct method (2^{-ΔΔCt}). All qPCR analyses were performed in triplicate using three independent biological replicates.

Stomatal aperture analysis. Detached leaves of Arabidopsis seedlings were treated with various buffers as indicated. Epidermal peels were mounted on a slide glass, and photographs of the abaxial leaf surface were captured using a Nikon Eclipse i80 microscope equipped with a camera (Nikon). The width and length of the stomatal aperture were measured using Fiji software, and the stomatal aperture index was calculated by dividing the aperture width by the length⁷⁹.

Statistics and reproducibility. All statistical analyses were conducted using R version 4.0.3⁸⁰ and Microsoft Excel. The analysis included a two-sample t-test, Wilcoxon rank-sum test, and one-way or two-way analysis of variance (ANOVA) with Tukey's HSD. Each experiment was performed at least three times.

Reporting summary. Further information on research design is available in the Nature Portfolio Reporting Summary linked to this article.

Data availability

All data presented in this study are included in the main text and Supplementary Information. All source data of the main figures are included in the Supplementary Data 1. Uncropped blot images of Supplementary Fig. 8 are shown in Supplementary Fig. 9. Any additional data and plants are available upon reasonable request.

Code availability

The scripts used for the pH analysis (dual excitation ratio values and its calibration to the absolute pH) are available at https://github.com/SeoyeonCha/pH_analysis.

Received: 27 March 2023; Accepted: 23 January 2024;

Published online: 05 February 2024

References

1. Lawson, T. & Matthews, J. Guard cell metabolism and stomatal function. *Annu. Rev. Plant Biol.* **71**, 273–302 (2020).
2. Dubeaux, G. et al. Deep dive into CO₂-dependent molecular mechanisms driving stomatal responses in plants. *Plant Physiol.* **187**, 2032–2042 (2021).
3. Kim, T. H., Böhmer, M., Hu, H., Nishimura, N. & Schroeder, J. I. Guard cell signal transduction network: advances in understanding abscisic acid, CO₂, and Ca²⁺ signaling. *Annu. Rev. Plant Biol.* **61**, 561–591 (2010).
4. Schroeder, J. I., Raschke, K. & Neher, E. Voltage dependence of K⁺ channels in guard-cell proto-plasts. *Proc. Natl. Acad. Sci.* **84**, 4108–4112 (1987).
5. Zhang, J. et al. Identification of slac1 anion channel residues required for co₂/bicarbonate sensing and regulation of stomatal movements. *Proc. Natl. Acad. Sci.* **115**, 11129–11137 (2018).
6. Wang, Y. et al. Systems dynamic modeling of a guard cell Cl⁻ channel mutant uncovers an emergent homeostatic network regulating stomatal transpiration. *Plant Physiol.* **160**, 1956–1967 (2012).
7. Mao, J., Zhang, Y. C., Sang, Y., Li, Q. H. & Yang, H. Q. A role for arabidopsis cryptochromes and cop1 in the regulation of stomatal opening. *Proc. Natl. Acad. Sci.* **102**, 12270–12275 (2005).

8. Kang, C. Y., Lian, H. L., Wang, F. F., Huang, J. R. & Yang, H. Q. Cryptochromes, phytochromes, and cop1 regulate light-controlled stomatal development in arabidopsis. *Plant Cell* **21**, 2624–2641 (2009).
9. Lee, J. H., Jung, J. H. & Park, C. M. Light inhibits cop1-mediated degradation of ice transcription factors to induce stomatal development in arabidopsis. *Plant Cell* **29**, 2817–2830 (2017).
10. Han, X., Huang, X. & Deng, X. W. The photomorphogenic central repressor cop1: conservation and functional diversification during evolution. *Plant Commun.* **1**, 100044 (2020).
11. Osterlund, M. T., Hardtke, C. S., Wei, N. & Deng, X. W. Targeted destabilization of hy5 during light-regulated development of arabidopsis. *Nature* **405**, 462–466 (2000).
12. Seo, H. S. et al. Lf1 ubiquitination by cop1 controls photomorphogenesis and is stimulated by spa1. *Nature* **423**, 995–999 (2003).
13. Jang, I. C., Yang, J. Y., Seo, H. S. & Chua, N. H. Hfr1 is targeted by cop1 e3 ligase for post-translational proteolysis during phytochrome a signaling. *Genes Dev.* **19**, 593–602 (2005).
14. Liu, L. J. et al. Cop1-mediated ubiquitination of constans is implicated in cryptochrome regulation of flowering in arabidopsis. *Plant Cell* **20**, 292–306 (2008).
15. Wang, W., Chen, Q., Botella, J. R. & Guo, S. Beyond light: insights into the role of constitutively photomorphogenic1 in plant hormonal signaling. *Front. Plant Sci.* **10**, 557 (2019).
16. Yu, J. W. et al. Cop1 and elf3 control circadian function and photoperiodic flowering by regulating gi stability. *Mol. Cell* **32**, 617–630 (2008).
17. Chen, Q. et al. Cop1 promotes aba-induced stomatal closure by modulating the abundance of abi/hab and ahg3 phosphatases. *New Phytol.* **229**, 2035–2049 (2021).
18. Wang, F. F., Lian, H. L., Kang, C. Y. & Yang, H. Q. Phytochrome b is involved in mediating red light-induced stomatal opening in arabidopsis thaliana. *Mol. Plant* **3**, 246–259 (2010).
19. Tossi, V., Lamattina, L., Jenkins, G. I. & Cassia, R. O. Ultraviolet-b-induced stomatal closure in arabidopsis is regulated by the uv resistance locus8 photoreceptor in a nitric oxide-dependent mechanism. *Plant Physiol.* **164**, 2220–2230 (2014).
20. Ge, X. M. et al. UV resistance locus8 mediates ultraviolet-b-induced stomatal closure in an ethylene-dependent manner. *Plant Sci.* **301**, 110679 (2020).
21. Khanna, R. et al. Cop1 jointly modulates cytoskeletal processes and electrophysiological responses required for stomatal closure. *Mol. Plant* **7**, 1441–1454 (2014).
22. Ma, Y. et al. Regulators of pp2c phosphatase activity function as abscisic acid sensors. *Science* **324**, 1064–1068 (2009).
23. Li, J., Wang, X. Q., Watson, M. B. & Assmann, S. M. Regulation of abscisic acid-induced stomatal closure and anion channels by guard cell aapk kinase. *Science* **287**, 300–303 (2000).
24. Brandt, B. et al. Reconstitution of abscisic acid activation of slac1 anion channel by cpk6 and ost1 kinases and branched abi1 pp2c phosphatase action. *Proc. Natl. Acad. Sci.* **109**, 10593–10598 (2012).
25. Imes, D. et al. Open stomata 1 (ost 1) kinase controls r-type anion channel quac 1 in a rabinidopsis guard cells. *Plant J.* **74**, 372–382 (2013).
26. Kinoshita, T. et al. Phot1 and phot2 mediate blue light regulation of stomatal opening. *Nature* **414**, 656–660 (2001).
27. Li, L. et al. Cell surface and intracellular auxin signalling for h⁺ fluxes in root growth. *Nature* **599**, 273–277 (2021).
28. Yang, J. et al. Tmk1-based auxin signaling regulates abscisic acid responses via phosphorylating abi1/2 in arabidopsis. *Proc. Natl. Acad. Sci.* **118**, e2102544118 (2021).
29. Schaller, A. & Oecking, C. Modulation of plasma membrane h⁺-atpase activity differentially activates wound and pathogen defense responses in tomato plants. *Plant Cell* **11**, 263–272 (1999).
30. Lee, H. Y. et al. Plasma membrane-localized plant immune receptor targets h⁺-atpase for membrane depolarization to regulate cell death. *New Phytol.* **233**, 934–947 (2022).
31. Merlot, S. et al. Constitutive activation of a plasma membrane h⁺-atpase prevents abscisic acid-mediated stomatal closure. *EMBO J.* **26**, 3216–3226 (2007).
32. Pei, D. et al. Phosphorylation of the plasma membrane h⁺-atpase aha2 by bak1 is required for aba-induced stomatal closure in arabidopsis. *Plant Cell* **34**, 2708–2729 (2022).
33. Irving, H. R., Gehring, C. A. & Parish, R. W. Changes in cytosolic ph and calcium of guard cells precede stomatal movements. *Proc. Natl. Acad. Sci.* **89**, 1790–1794 (1992).
34. Li, K. et al. An optimized genetically encoded dual reporter for simultaneous ratio imaging of ca²⁺ and h⁺ reveals new insights into ion signaling in plants. *New Phytol.* **230**, 2292–2310 (2021).
35. Demes, E. et al. Dynamic measurement of cytosolic ph and [no₃⁻] uncovers the role of the vacuolar transporter ATCLCA in cytosolic ph homeostasis. *Proc. Natl. Acad. Sci.* **117**, 15343–15353 (2020).
36. Andrés, Z. et al. Control of vacuolar dynamics and regulation of stomatal aperture by tonoplast potassium uptake. *Proc. Natl. Acad. Sci.* **111**, E1806–E1814 (2014).
37. Bak, G. et al. Rapid structural changes and acidification of guard cell vacuoles during stomatal closure require phosphatidylinositol 3, 5-bisphosphate. *Plant Cell* **25**, 2202–2216 (2013).
38. Liu, J., Ji, Y., Zhou, J. & Xing, D. Phosphatidylinositol 3-kinase promotes v-atpase activation and vacuolar acidification and delays methyl jasmonate-induced leaf senescence. *Plant Physiol.* **170**, 1714–1731 (2016).
39. Zhang, H. et al. Rnai-directed downregulation of vacuolar h⁺-atpase subunit a results in enhanced stomatal aperture and density in rice. *PLoS One* **8**, e69046 (2013).
40. Kim, J. Y. et al. Cop1 mutation causes low leaf temperature under various abiotic stresses in arabidopsis thaliana. *Plant Direct* **6**, e473 (2022).
41. Segami, S., Makino, S., Miyake, A., Asaoka, M. & Maeshima, M. Dynamics of vacuoles and h⁺-pyrophosphatase visualized by monomeric green fluorescent protein in arabidopsis: artifactual bulbs and native intravacuolar spherical structures. *Plant Cell* **26**, 3416–3434 (2014).
42. Krebs, M. et al. Arabidopsis v-atpase activity at the tonoplast is required for efficient nutrient storage but not for sodium accumulation. *Proc. Natl. Acad. Sci.* **107**, 3251–3256 (2010).
43. Li, J. et al. Arabidopsis h⁺-ppase avp1 regulates auxin-mediated organ development. *Science* **310**, 121–125 (2005).
44. Martinoia, E., Maeshima, M. & Neuhaus, H. E. Vacuolar transporters and their essential role in plant metabolism. *J. Exp. Bot.* **58**, 83–102 (2007).
45. Ferjani, A. et al. Keep an eye on ppi: the vacuolar-type h⁺-pyrophosphatase regulates post-germinative development in arabidopsis. *Plant Cell* **23**, 2895–2908 (2011).
46. Kurkdjian, A. & Guern, J. Intracellular ph: measurement and importance in cell activity. *Annu. Rev. Plant Biol.* **40**, 271–303 (1989).
47. Barbez, E., Dünser, K., Gaidora, A., Lendl, T. & Busch, W. Auxin steers root cell expansion via apoplastic ph regulation in arabidopsis thaliana. *Proc. Natl. Acad. Sci.* **114**, E4884–E4893 (2017).
48. Felle, H. H., Hanstein, S., Steinmeyer, R. & Hedrich, R. Dynamics of ionic activities in the apoplast of the sub-stomatal cavity of intact vicia faba leaves during stomatal closure evoked by aba and darkness. *Plant J.* **24**, 297–304 (2000).
49. Geilfus, C. M. The ph of the apoplast: dynamic factor with functional impact under stress. *Mol. Plant* **10**, 1371–1386 (2017).
50. McNellis, T. W., Von Arnim, A. G. & Deng, X. W. Overexpression of arabidopsis cop1 results in partial suppression of light-mediated development: evidence for a light-inactivable repressor of photomorphogenesis. *Plant Cell* **6**, 1391–1400 (1994).
51. Qiu, Q. S., Guo, Y., Dietrich, M. A., Schumaker, K. S. & Zhu, J. K. Regulation of SOS1, a plasma membrane Na⁺/H⁺ exchanger in Arabidopsis thaliana, by SOS₂ and SOS₃. *Proc. Natl. Acad. Sci. USA* **99**, 8436–8441 (2002).
52. Yang, Y. et al. The Arabidopsis chaperone J3 regulates the plasma membrane H⁺-ATPase through interaction with the PKS5 kinase. *Plant Cell* **22**, 1313–1332 (2010).
53. Gévaudant, F. et al. Expression of a constitutively activated plasma membrane H⁺-ATPase alters plant development and increases salt tolerance. *Plant Physiol.* **144**, 1763–1776 (2007).
54. Yang, Y. et al. The Ca²⁺ sensor SCaBP3/CBL7 modulates plasma membrane H⁺-ATPase activity and promotes alkali tolerance in arabidopsis. *Plant Cell* **31**, 1367–1384 (2019).
55. Kim, J. Y. et al. Cop1 controls salt stress tolerance by modulating sucrose content. *Plant Signal. Behav.* **17**, 2096784 (2022).
56. Lin, W. et al. Tmk-based cell-surface auxin signalling activates cell-wall acidification. *Nature* **599**, 278–282 (2021).
57. Netting, A. ph, abscisic acid and the integration of metabolism in plants under stressed and non-stressed conditions: cellular responses to stress and their implication for plant water relations. *J. Exp. Bot.* **51**, 147–158 (2000).
58. Xue, Y., Yang, Y., Yang, Z., Wang, X. & Guo, Y. VAMP711 is required for abscisic acid-mediated inhibition of plasma membrane H⁺-ATPase activity. *Plant Physiol.* **178**, 1332–1343 (2018).
59. Wang, Y. et al. Overexpression of plasma membrane h⁺-atpase in guard cells promotes light-induced stomatal opening and enhances plant growth. *Proc. Natl. Acad. Sci.* **111**, 533–538 (2014).
60. Park, Y. J., Lee, H. J., Ha, J. H., Kim, J. Y. & Park, C. M. Cop 1 conveys warm temperature information to hypocotyl thermomorphogenesis. *New Phytol.* **215**, 269–280 (2017).
61. Lian, N. et al. Cop1 mediates dark-specific degradation of microtubule-associated protein wdl3 in regulating arabidopsis hypocotyl elongation. *Proc. Natl. Acad. Sci.* **114**, 12321–12326 (2017).
62. Smardon, A. M. & Kane, P. M. Loss of vacuolar h⁺-atpase activity in organelles signals ubiquitination and endocytosis of the yeast plasma membrane proton pump pma1p. *J. Biol. Chem.* **289**, 32316–32326 (2014).

63. Kerkeb, L., Venema, K., Donaire, J. P. & Rodríguez-Rosales, M. P. Enhanced h^+ /atp coupling ratio of h^+ -atpase and increased 14-3-3 protein content in plasma membrane of tomato cells upon osmotic shock. *Physiol. Plant.* **116**, 37–41 (2002).
64. Takemiya, A. & Shimazaki, K. Phosphatidic acid inhibits blue light-induced stomatal opening via inhibition of protein phosphatase 1. *Plant Physiol.* **153**, 1555–1562 (2010).
65. Takemiya, A. et al. KI Shimazaki. Phosphorylation of BLUS1 kinase by phototropins is a primary step in stomatal opening. *Nat. Commun.* **4**, 2094 (2013).
66. Inoue, S. et al. Blue light-induced autophosphorylation of phototropin is a primary step for signaling. *Proc. Natl Acad. Sci. USA* **105**, 5626–5631 (2008).
67. Pandey, S., Zhang, W. & Assmann, S. M. Roles of ion channels and transporters in guard cell signal transduction. *FEBS Lett.* **581**, 2325–2336 (2007).
68. Amtmann, A., Jelitto, T. C. & Sanders, D. K^+ -Selective inward-rectifying channels and apoplastic pH in barley roots. *Plant Physiol.* **120**, 331–338 (1999).
69. Rayle, D. L. & Cleland, R. Enhancement of wall loosening and elongation by acid solutions. *Plant Physiol.* **46**, 250–253 (1970).
70. Hager, A. Role of the plasma membrane h^+ -atpase in auxin-induced elongation growth: historical and new aspects. *J. Plant Res.* **116**, 483–505 (2003).
71. Rienmüller, F. et al. Luminal and cytosolic pH feedback on proton pump activity and ATP affinity of V-type ATPase from Arabidopsis. *J. Biol. Chem.* **287**, 8986–8993 (2012).
72. Takahashi, K., Hayashi, K. & Kinoshita, T. Auxin activates the plasma membrane H^+ -ATPase by phosphorylation during hypocotyl elongation in Arabidopsis. *Plant Physiol.* **159**, 632–641 (2012).
73. MacRobbie, E. A. Evidence for a role for protein tyrosine phosphatase in the control of ion release from the guard cell vacuole in stomatal closure. *Proc. Natl Acad. Sci. USA* **99**, 11963–11968 (2002).
74. Monden, K. et al. Root-specific activation of plasma membrane H^+ -ATPase 1 enhances plant growth and shoot accumulation of nutrient elements under nutrient-poor conditions in Arabidopsis thaliana. *Biochem. Biophys. Res. Commun.* **621**, 39–45 (2022).
75. Schöniche, A., Webb, B. A., Jacobson, M. P. & Barber, D. L. Considering protonation as a posttranslational modification regulating protein structure and function. *Annu. Rev. Biophys.* **42**, 289–314 (2013).
76. Chen, Z. H. et al. Molecular evolution of grass stomata. *Trends Plant Sci.* **22**, 124–139 (2017).
77. Webb, B. A., Chimenti, M., Jacobson, M. P. & Barber, D. L. Dysregulated pH: a perfect storm for cancer progression. *Nat. Rev. Cancer* **11**, 671–677 (2011).
78. McNellis, T. W. et al. Genetic and molecular analysis of an allelic series of cop1 mutants suggests functional roles for the multiple protein domains. *Plant Cell* **6**, 487–500 (1994).
79. Eisele, J. F., Fäßler, F., Bürgel, P. F. & Chaban, C. A rapid and simple method for microscopy-based stomata analyses. *PLoS One* **11**, e0164576 (2016).
80. R Core Team, R: A Language and Environment for Statistical Computing (R Foundation for Statistical Computing, Vienna, Austria), (2022).

Acknowledgements

This work was supported by the National Research Foundation of Korea (NRF) grant funded by the Korean government (MSIT) (Project No. 2021R1A2C1003446).

Author contributions

H.S.S. designed research; S.C. and W.K.M. performed research; S.C., W.K.M., and H.S.S. analyzed data; and S.C., W.K.M., and H.S.S. wrote the paper.

Competing interests

The authors declare no competing interests.

Additional information

Supplementary information The online version contains supplementary material available at <https://doi.org/10.1038/s42003-024-05847-w>.

Correspondence and requests for materials should be addressed to Hak Soo Seo.

Peer review information *Communications Biology* thanks Chun-Peng Song, Yusuke Aihara, and Jun-Min He for their contribution to the peer review of this work. Primary Handling Editor: David Favero. A peer review file is available.

Reprints and permission information is available at <http://www.nature.com/reprints>

Publisher's note Springer Nature remains neutral with regard to jurisdictional claims in published maps and institutional affiliations.



Open Access This article is licensed under a Creative Commons Attribution 4.0 International License, which permits use, sharing, adaptation, distribution and reproduction in any medium or format, as long as you give appropriate credit to the original author(s) and the source, provide a link to the Creative Commons licence, and indicate if changes were made. The images or other third party material in this article are included in the article's Creative Commons licence, unless indicated otherwise in a credit line to the material. If material is not included in the article's Creative Commons licence and your intended use is not permitted by statutory regulation or exceeds the permitted use, you will need to obtain permission directly from the copyright holder. To view a copy of this licence, visit <http://creativecommons.org/licenses/by/4.0/>.

© The Author(s) 2024